CONSTITUTIVE MODELING OF CARBON FIBER FABRIC: FROM MATERIAL PARAMETER IDENTIFICATION TO APPLICATION IN FE FORMING SIMULATION

Masato Nishi[1], Ichiro Taketa[2], Akira Iwata[3] and Tei Hirashima[4]

[1]Engineering Technology Division, JSOL Corporation, 2-5-24, Harumi, Chuo-ku, Tokyo, Japan
Email: nishi.masato@jsol.co.jp, Web Page: http://www.jsol.co.jp/english/cae/
[2]Composite Materials Research Laboratories, Toray Industries, Inc.,
1515 Tsutsui Masaki-cho Iyogun, Ehime, Japan
Email: Ichiro_Taketa@nts.toray.co.jp, web page: http://www.toray.com/
[3] Engineering Development Center, Toray Industries, Inc.,
3-1, Sonoyama 3-chome, Otsu, Shiga, Japan
Email: Akira_Iwata@nts.toray.co.jp, web page: http://www.toray.com/
[4]Engineering Technology Division, JSOL Corporation, 2-2-4 Tosabori, Nishi-ku, Osaka, Japan
Email: hirashima.tei@jsol.co.jp, Web Page: http://www.jsol.co.jp/english/cae/

Keywords: carbon fiber fabric, finite element analysis, forming, parameter identification, wrinkle

Abstract
Many of the existing finite element models in macroscopic forming simulation of carbon fiber fabric have neglected out-of-plane bending stiffness by using membrane elements. To consider this, some models proposed in recent studies can capture the bending stiffness as a bending virtual work separately from in-plane deformation. The shell-membrane hybrid model proposed in the author's previous study also deals with bending stiffness as a function of the rotation of mid-surface. However, influence of the transverse shear deformation upon the bending behavior is not able to be described in these models. In this study, in order to simulate the transverse shear deformation robustly, the thick-shell model based on Reissner-Mindlin plate theory is applied in the forming simulation. To compare the predictive capability of out-of-plane deformation, especially wrinkling, by the thick-shell model to the conventional shell-membrane hybrid model, we identify the material parameters of each model through a series of coupon experiments. After that, the forming simulations are carried out by these two models and verified by means of comparison with the actual experimental deformations. Small wrinkles observed in the forming experiment are not represented in the shell-membrane hybrid model, but can be captured in the thick-shell model.

1. Introduction

The forming process of carbon fiber reinforced plastic has increased its presence in the industry due to its wide applicability to mass production. Finite element (FE) simulation is effective in optimizing process conditions, and minimizing lead times and design costs. Dominant deformation modes of carbon fiber fabric during forming are in-plane shear and out-of-plane bending due to high deformability. In particular, bending behavior affects the onset and formation of wrinkles, which is one of the major forming defects. Therefore accurate description of bending behavior is an important aspect in the accurate prediction of wrinkling.

Many of the existing FE models [1-4] in macroscopic forming simulation of carbon fiber fabric have neglected out-of-plane bending stiffness, by using membrane elements, as it is very low compared to

Excerpt from ISBN 978-3-00-053387-7

in-plane stiffness. To consider this, some FE models proposed in recent studies [5, 6] can capture out-of-plane bending stiffness as a bending virtual work separately from in-plane deformation. The shell-membrane hybrid model (S-M model) proposed in the author's previous study [7, 8] also deals with bending stiffness as a function of the rotation of the mid-surface by using the feature for moving the shell reference surface from the mid-surface in LS-DYNA® [9]. However, influence of transverse shear deformation upon bending behavior is not able to be described by these models.

In order to simulate transverse shear deformation robustly, the thick-shell model (TS model) is applied in forming simulation in this study. The predictive capability of out-of-plane deformation, especially wrinkling, by the TS model is examined by comparing it to the conventional S-M model, in which out-of-plane bending behavior is simulated independently of in-plane behavior and does not consider transverse shear deformation. The starting point of this study is material parameter identification in each model through a series of coupon experiments. In the S-M model, the non-linear bending properties are derived from 3-point bending tests across yarn and in a 45° direction. On the other hand, the transverse shear modulus is derived from 3-point bending tests with the in-plane properties because the bending behavior results from the combination of the mid-surface rotation and the transverse shear deformation in the TS model. Furthermore, the non-linear bending behavior is described by adjusting the in-plane compressive property to be asymmetric to the tensile property. To complete the study, forming simulations are carried out using these two FE models and verified by means of comparison with the actual deformations in forming experiment. Then we evaluate the prediction capability of bending behavior in each model. Small wrinkles observed in the forming experiment are not represented in the shell-membrane hybrid model, but can be captured in the thick-shell model.

2. Constitutive modeling

2.1. Shell-Membrane hybrid model (S-M model)

The constitutive modeling of the S-M model is shown in Fig.1.. In-plane properties are described by the membrane element and the bending stiffness is represented by a set of elements which consist of two shell elements with the membrane element in between. It is assumed that the out-of-plane moment is decoupled from the in-plane stress [7, 8].

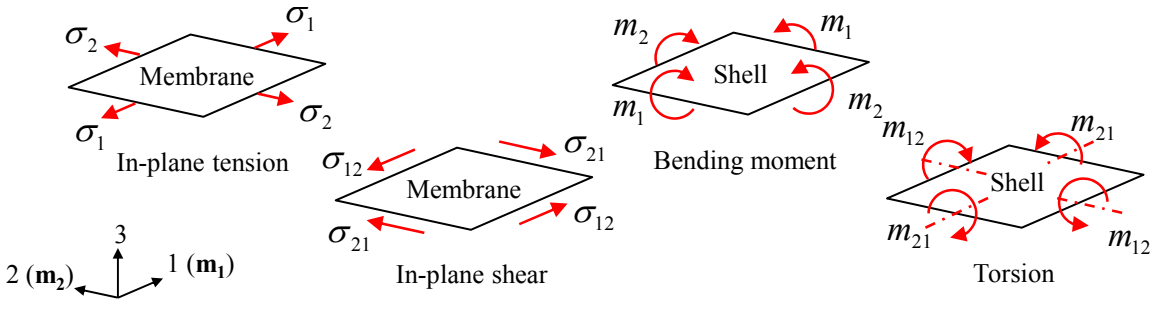

Figure 1. Constitutive modeling of S-M model.

By using Kirchhoff-Love's (Euler-Bernoulli) assumption [10] that does not take into account transverse shear deformation, a bending deflection $v(x)$ for the 3-point bending boundary condition represented in the S-M model is described as follow.

$$v(x) = \frac{P}{12EI} \cdot x \cdot \left(\frac{3}{4} l^2 - x^2 \right) \tag{1}$$

Excerpt from ISBN 978-3-00-053387-7

where P is a load at the center point, EI is bending stiffness, and l is the length between bearings. In this assumption, the cross section remains normal to the mid-surface under the out-of-plane bending deformation as shown in Fig. 2.

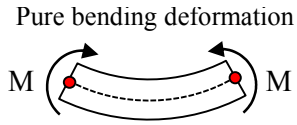

Figure 2. Out-of-plane deformation of S-M model.

An anisotropic hyperelastic model which independently calculates tension in the yarn directions and in-plane shear for simulating and considers yarn reorientation under the large shear deformation is introduced into the membrane element in the S-M model to describe the in-plane behaviors. Stresses due to elongation of the individual yarn families are then computed as the sum:

$$\boldsymbol{\sigma} = \sum_{i=1}^{n} \frac{1}{J} \cdot f(\varepsilon_i) \cdot \mathbf{F} \cdot \left(\mathbf{m}_i^0 \otimes \mathbf{m}_i^0\right) \cdot \mathbf{F}^T \tag{2}$$

where $\mathbf{m}_i^0$ is an initial yarn direction, and current configuration is given as $\mathbf{m}_i = \mathbf{F}\mathbf{m}_i^0$. $\mathbf{F}$ and $\boldsymbol{J}$ are the deformation gradient tensor and the Jacobian of the deformation, respectively. f is a function to denote the relationship between stress and strain in yarn direction.
Interaction between neighboring yarn families can be accounted for by:

$$\boldsymbol{\sigma} = \sum_{\substack{i,j \\ i \neq j}} \frac{1}{J} \cdot g(\gamma_{ij}) \cdot \mathbf{F} \cdot \left(\mathbf{m}_i^0 \otimes \mathbf{m}_j^0\right) \cdot \mathbf{F}^T \tag{3}$$

where g is a function to denote the relationship between in-plane shear stress and in-plane shear strain.

2.2. Thick-Shell model (TS model)

The TS model based on Reissner-Mindlin plate theory [11] can simulate transverse shear deformation as shown in Fig.3.

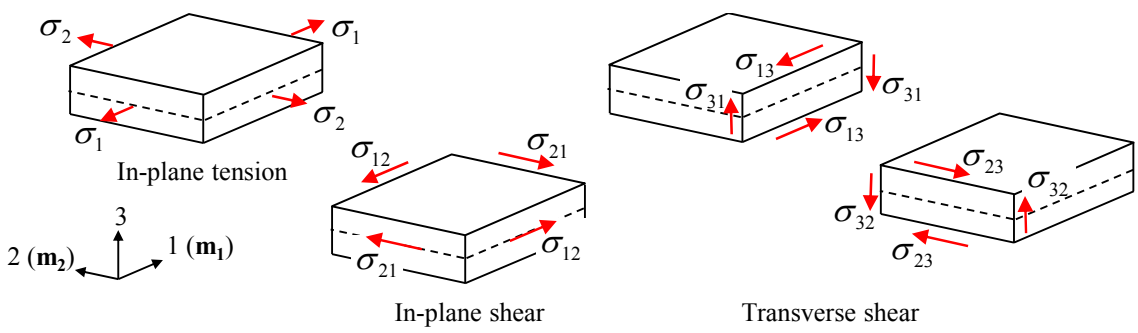

Figure 3. Constitutive modeling of TS model.

A bending deflection $v(x)$ under a 3-point bending boundary condition in TS model is described by using the Reissner-Mindlin (Timoshenko) assumption. The mid-surface displacement plus rotations

Excerpt from ISBN 978-3-00-053387-7

are allowed to describe the transverse shear deformation. It is described by Eq.4.

$$v(x) = v_b(x) + v_s(x) = \frac{P}{12EI} \cdot x \cdot \left(\frac{3}{4} l^2 - x^2 \right) + \frac{\alpha \cdot P \cdot x}{2G \cdot A} \tag{4}$$

where $v_b(x)$ and $v_s(x)$ are the deflection due to pure bending deformation and the deflection due to transverse shear deformation, respectively. α is the shear correction factor and A is the cross section area. Eq. 4 shows that the out-of-plane deformation in the TS model represents two deformation modes. One is the pure bending expressed in first term, and the other is the transverse shear deformation expressed in second term, as shown in Fig. 4.
An anisotropic hyperelastic model is also applied to the thick-shell element to deal with a large in-plane shear deformation.

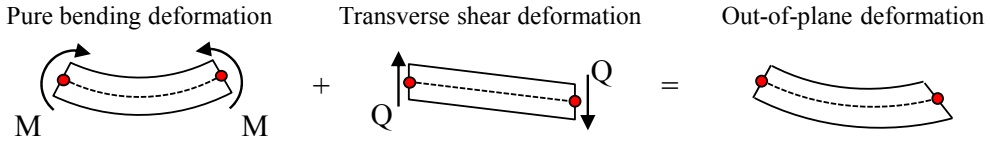

Figure 4. Out-of-plane deformation of TS model.

3. Parameter identification

In this section, the identification processes for material parameters in the S-M model and the TS model will be discussed. A plain-weave carbon fiber fabric (T300-3K, Toray) with a thickness of 0.23 mm is used in this study. Each parameter in each model is identified through a series of coupon tests, uniaxial tension across yarn direction, bias-extension and 3-point bending tests, as shown in Fig. 5.

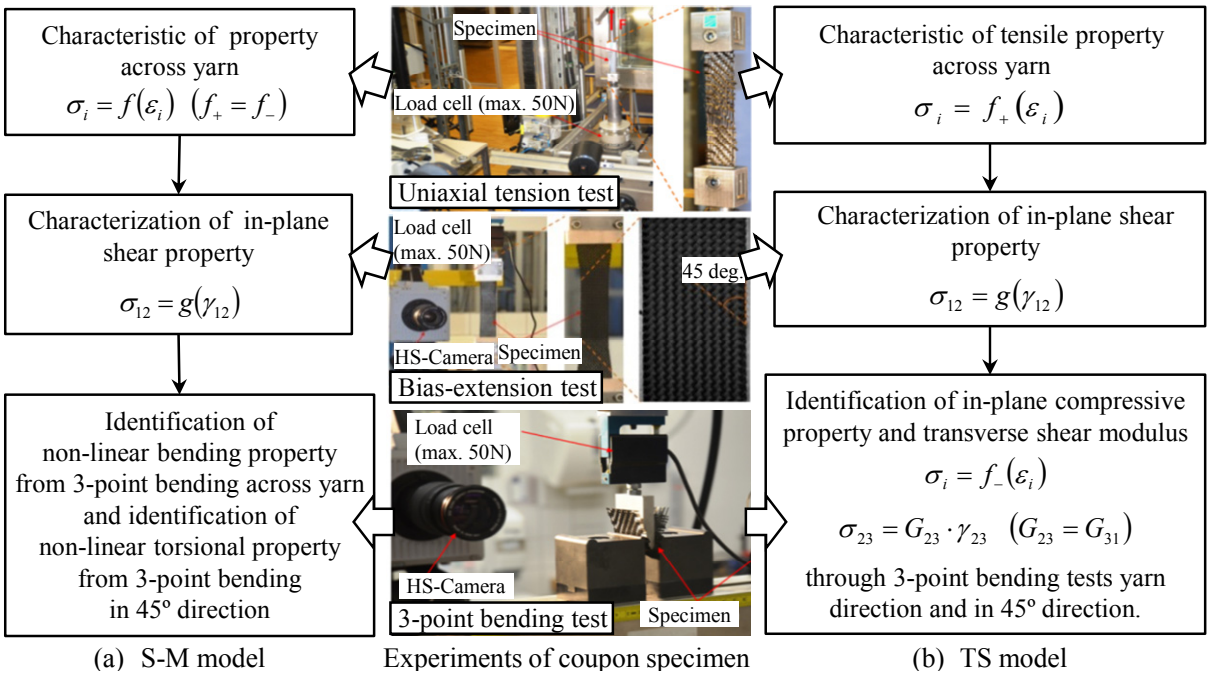

Figure 5. Identification process of material parameters through coupon experiments.

Excerpt from ISBN 978-3-00-053387-7

Stress–strain relationship in yarn direction *f* is obtained from a uniaxial tension test across yarn direction. The specimen is rectangular with a free clamping length of 80 mm and a width of 24 mm. During the uniaxial tension test, the force is measured by a load cell (max. 10 kN) and the displacement is measured optically by a high-speed camera. In the S-M model, a compressive stress–strain relationship is assumed as being symmetric to the tensile property.

In-plane shear stress–shear strain relationship *g* is obtained from a bias-extension test. The dimension of the bias-extension test specimen is a free clamping length of 120 mm and a width of 30 mm with a ratio of length to width of 4:1. During the bias-extension test, displacement and force history are recorded. The load is measured by a load cell (max. 50N). If the yarns are considered inextensible and no intra-ply slip occurs within the specimen (correlation with the Pin Jointed Net assumption [12]), shear angle γ_{12} and shear stress σ_{12} are calculated as follows.

$$\gamma_{12} = \frac{\pi}{2} - 2\arccos\left(\frac{H - W + d}{\sqrt{2}(H - W)}\right) \tag{5}$$

$$\sigma_{12}(\gamma_{12}) = \frac{1}{(2H - 3W)\cdot t\cdot\cos\gamma_{12}}\left(\left(\frac{H}{W} - 1\right)\cdot F\cdot\left(\cos\frac{\gamma_{12}}{2} - \sin\frac{\gamma_{12}}{2}\right) - W\cdot\sigma_{12}\left(\frac{\gamma_{12}}{2}\right)\cdot\cos\frac{\gamma_{12}}{2}\cdot t\right) \tag{6}$$

where *F* and *d* are the load cell force and the applied displacement of the crosshead of the testing, respectively. *H*, *W* and *t* are the length, width and thickness of specimen.

Out-of-plane material parameters are identified from 3-point bending tests as shown in Fig. 6 (a). The bending specimens are quadratic with a size of 40 mm. During the bending tests, displacement and force histories are recorded. The force is measured by a load cell (max. 50N). The displacement of the center of the specimen is determined by the displacement of the crosshead of the testing machine. By the use of beam theory, the relationship between moment and cavature for the S-M model is derived from measured displacement and force history in yarn direction and the torsional relationship is calculated from the bending test in 45˚ direction as well.

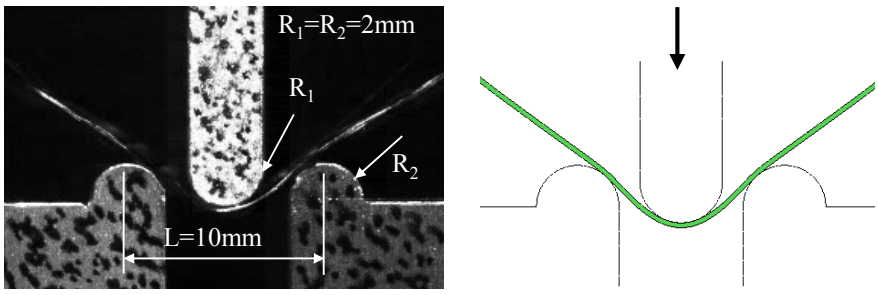

(a) Experiment (b) TS model

Figure 6. Deformations under 3-point bending along yarn direction.

Fig. 6 (b) shows the deformation in the TS model under 3-point bending condition. Transverse shear modulus G_{23} (=G_{31}) and the compressive property in yarn directions *f*. in the TS model are identified by fitting the experimental results of the 3-point bending tests in yarn and 45˚ directions. An optimization tool LS-OPT® [13] is used. The resultant force–displacement curves converged in 4 iterations using the mean squared error method. Fig. 7 shows the optimized histories.

Excerpt from ISBN 978-3-00-053387-7

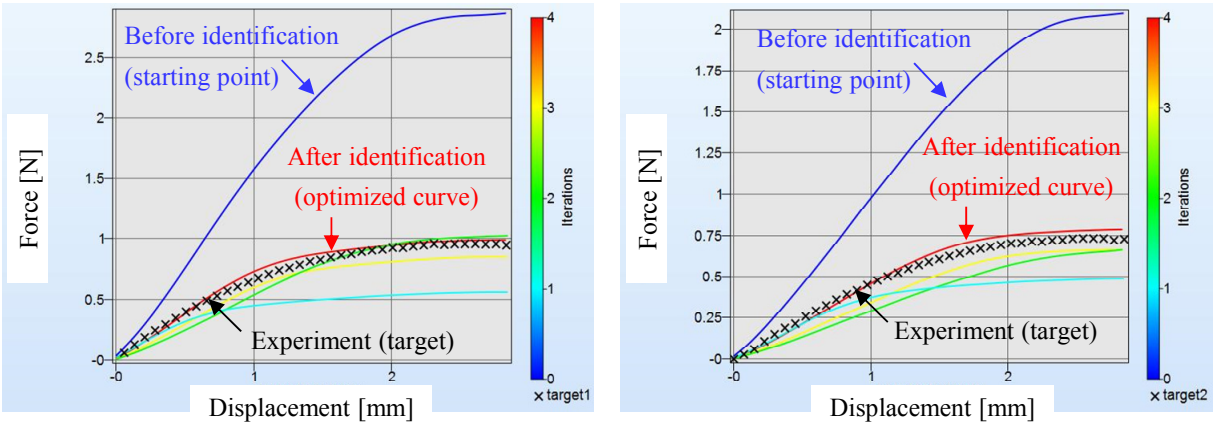

(a) Along yarn direction (b) 45˚ direction

Figure 7. Out-of-plane responses under 3-point bending at various iterations in LS-OPT.

The very small value for G_{23} (=G_{31}) in the TS model has been identified from the 3-point bending tests. It is clear from Eq. 4 that the ratio of the transverse shear deflection $v_s(x)$ to the bending deflection $v_b(x)$ increases under the shorter length between bearings. This suggests that the predictable possibility for a small wrinkle, which is difficult to predict in the conventional FE model like the S-M model, increases in the TS model since this accounts for transverse shear deformation.

4. Forming simulation

Forming simulations are performed by using the identified parameters in both the S-M model and the TS model, and compared to the experimental deformations including the wrinkling during the forming process. A schematic figure of the FE model is shown in Fig. 8. The blank size is 280 × 280 mm. It is meshed with 313,600 elements. The surface of upper and lower forming tools are modeled as rigid bodies. The carbon fiber fabric is in tension during the forming process by gripping it at 4 corners. The downward movement of upper tool is 20 mm.

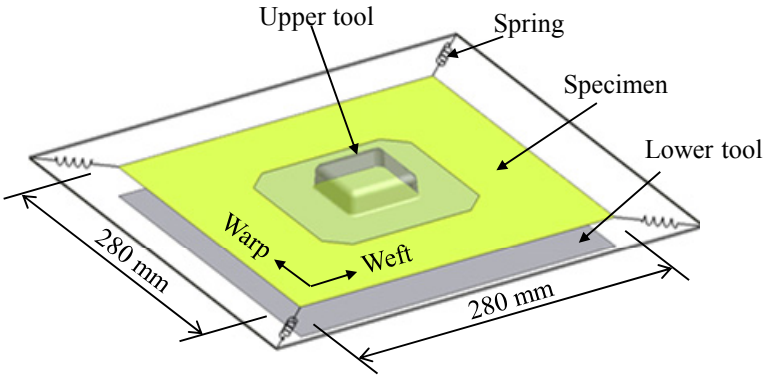

Figure 8. FE model of square tube forming.

Fig. 9 shows the top view of the deformation of the blank during the forming experiment. Wrinkles are observed around the corners and develop along with the movement of tool. A large and a small wrinkle are observed at 15 mm travel, 5 mm remaining closure travel, as shown in Fig. 9 (a). In the forming process, it is necessary to undergo in-plane deformation to conform the blank to the tool

Excerpt from ISBN 978-3-00-053387-7

geometry. A large in-plane shear deformation typically occurs during forming of a carbon fiber fabric since the in-plane shear resistance is very low until the shear locking angle. If the shear deformation reaches the locking angle, out-of-plane wrinkling occurs.

(a) 15 mm travel (5 mm remaining closure travel) (b) 20 mm travel (full mold)

Figure 9. Wrinkles observed during forming experiment.

Predictive deformations and distributions of shear angle at 15 mm travel by both the S-M model and the TS model, are shown in Fig. 10. In Fig. 10 (a), large wrinkles are actually present around the corners in the S-M model. These were also observed in the forming experiments, but the experiments showed small wrinkles between the large wrinkles as shown in Fig. 9 (b). As expected, small wrinkles are not represented in the S-M model. Fig. 10 (b) shows the simulated deformation in the TS model. The small wrinkles that are not captured in the S-M model can be captured in the TS model.

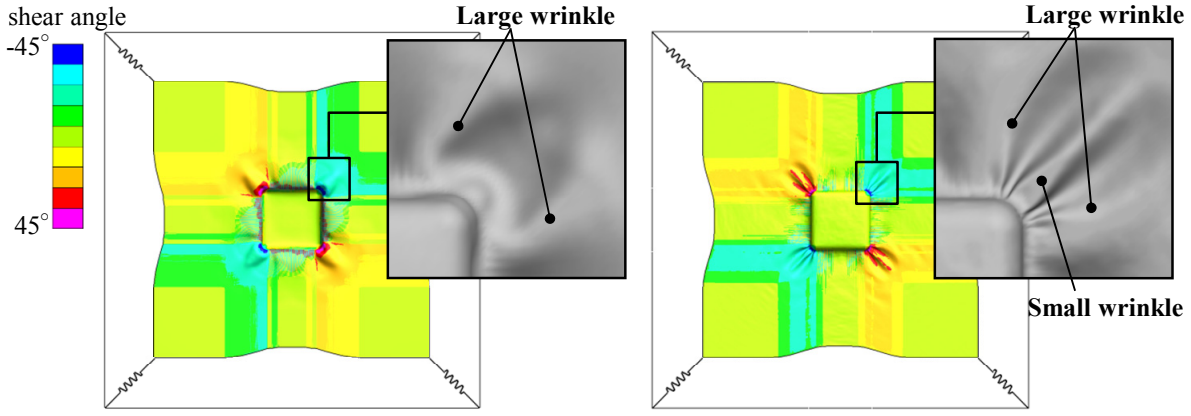

(a) S-M model (b) TS model

Figure 10. Wrinkles observed at 15 mm travel.

These simulation results demonstrate that when identifying bending stiffness, a conventional model which treats bending independently, like the S-M model, is insufficient to reproduce small wrinkling caused by transverse shear deformation. They also show that the TS model, which considers out-of-plane shear deformation, is an effective approach.

Excerpt from ISBN 978-3-00-053387-7

5. Conclusions

The influence of transverse shear deformation upon bending behavior, especially small wrinkling, was numerically examined in this paper. Forming simulations were carried out with two FE models, an S-M model and a TS model, and show that small wrinkles that were not captured in the S-M model were captured in the TS model. It has become clear that the small wrinkling is predominantly caused by transverse shear deformation.

Acknowledgments

The measurements of a series of coupon tests were conducted at Fraunhofer EMI and were guided by Dr. Matthias Boljen and Mr. Markus Jung. Their help is highly appreciated. The authors would like to thank Dr. Thomas Klöppel of DYNAmore for implementing new capabilities in LS-DYNA® to conduct the simulations in this study.

References

[1] P. Xue, X. Peng and J. Cao., A non-orthogonal constitutive model for characterizing woven composites, *Composites Part A: Applied Science and Manufacturing,* 34:183–193, 2003.
[2] A. Willems, S. V. Lomov, I. Verpoest, D. Vandepitte, P. Harrison and W. R. Yu, Forming simulation of a thermoplastic commingled woven textile on a double dome, *International Journal of Material Forming,* 1:965-968, 2008.
[3] R.H.W. ten Thije and R. Akkerman, A multi-layer triangular membrane finite element for the forming simulation of laminated composites, *Composites Part A: Applied Science and Manufacturing,* 40:739–753, 2009.
[4] Y. Aimene, E. Vidal-Sallé, B. Hagège, F. Sidoroff and P. Boisse, A hyperelastic approach for composite reinforcement large deformation analysis, *Journal of Composite Materials,* 44:5-26, 2010.
[5] P. Boisse, N. Hamila, E. Vidal-Sallé and F. Dumont, Simulation of wrinkling during textile composite reinforcement forming. Influence of tensile, in-plane shear and bending stiffnesses, *Composites Science and Technology,* 71:683–692, 2011.
[6] S.P. Haanappel, R.H.W. ten Thije, U. Sachs, B. Rietman and R. Akkerman, Formability analyses of uni-directional and textile reinforced thermoplastics, *Composites Part A: Applied Science and Manufacturing,* 56:80-92, 2014.
[7] M. Nishi, T. Hirashima and T. Kurashiki, Textile composite reinforcement forming analysis considering out-of-plane bending stiffness and tension dependent in-plane shear behavior, *Proceedings of the 16th European Conference on Composite Materials ECCM-16, Seville, Spain,* June 2014.
[8] M. Nishi and T. Hirashima, Forming simulation of textile composites using LS-DYNA, *Proceedings of the 10th European LS-DYNA Conference, Würzburg, Germany,* June 2015.
[9] J.O. Hallquist, *LS-DYNA Theory Manual*, Livermore Software Technology Corporation, 2006.
[10] G. Kirchhoff, Über das Gleichgewicht and die Bewegung einer elastischen Scheibe, *Journal für reine und angewandte Mathematik*, 40:51-88, 1850.
[11] R.D. Mindlin, Influence of rotatory inertia and shear on flexural motions of isotropic, elastic plates, J*ournal of Applied Mechanics*, 18:31-38, 1951.
[12] W. Lee, J. Padvoiskis, J. Cao, E. de Luycker, P. Boisse, F. Morestin, J. Chen and J. Sherwood, Bias-extension of woven composite fabrics, *International Journal of Material Forming*, 1:895-898, 2008
[13] N. Stander et al., *LS-OPT® 5.2 user's manual*, Livermore Software Technology Corporation, 2015.

Excerpt from ISBN 978-3-00-053387-7